Chapter 5

Gaussion Hartree Approximated Quantum Mechanics for Large-Scale Nonadiabatic Electron Dynamics

5.1 Introduction

Many chemical events, those where the nuclei move on a single potential energy surface (PES), can be simulated by quantum chemistry approaches with the assumption that electrons adjust instantaneously to the slower nuclear motion. With this assumption, which is called the Born-Oppenheimer (BO) approximation, the electronic component and the nuclear component of the wavefunction of the system can be decoupled mathematically. This forms the basis of the standard quantum chemistry methods.

However, there are also a large number of important processes in nature, such as photochemical and electrochemical reactions, that the PESs are close in energy and the nuclei transit between different PESs. During the transition, the motion of electrons and nuclei are strongly coupled, and the BO approximation breaks down. Such a transition is called a nonadiabatic transition, the theory for which was first proposed independently by Landau (*1*) and Zener (*2*) in 1932. A number of other approaches have been developed since then, including two mixed quantum-classical methods that are most widely adopted for nonadiabatic dynamics simulations, Ehrenfest dynamics (*3*–*6*) and surface hopping (*7*, *8*). Ehrenfest dynamics uses a mean-field approach in which the nuclei move on a single PES that averages over all quantum states, while the surface hopping method allows stochastic electronic transitions between states with the transition probability calculated using quantum mechanical or semiclassical methods. A number of variants of these methods have been developed, but they are still computationally demanding due to the use of advanced quantum chemistry methods to combine with these schemes, such as combining Ehrenfest dynamics with time-dependent Hartree Fock (TDHF) (*9*) or time-dependent density functional theory (TDDFT) (*10*), and the use of *ab initio* methods or TDDFT to compute the PESs for surface hopping. As many nonadiabatic phenomena happen in large systems, such as photosynthesis, etching of silicon, and insulator-to-metal transition of dense deuterium liquid, it is necessary to develop new methods to enable nonadiabatic dynamics simulations in large scale.

Aiming at solving this problem, Su et al. from our group have developed the electron force field (eFF)(*11*) framework for simulating large-scale nonadiabatic dynamics in condensed matter. In the eFF framework, the particles follow wave packet dynamics, with the nuclei represented by classical point charges propagated classically and electrons represented by wave packets. The use of wave packets relates to the perspective that, in systems that are highly excited with a high density of quasi-degenerate electronic states, there are continuous nonadiabatic transitions and large fluctuations of electronic states, which should be described by wave packets dynamics of electrons.(*12*)

Unlike the *ab initio* excited state dynamics methods which can only be realistic for hundreds of electrons on picosecond timescale, the eFF method expects to simulate hundreds of thousands of electrons on nanosecond timescale in a reasonable amount of time. It has been applied to studying problems including the shock Hugoniot curves of various materials,(*11*, *13*, *14*) Auger-induced chemistry,(*15*) Coulomb explosion in silicon and carbon,(*16*) and brittle fracture of silicon.(*17*) However, it bears certain shortcomings that inspired us to develop the Gaussion Hartree Approximated Quantum Mechanics (GHA-QM) method (*18*) based on its framework. A brief review of the eFF formulation and a discussion on the exploration and new improvements in GHA-QM are in the next sections.

5.2 The Electron Force Field (eFF) Framework

The eFF method relates to Fermion molecular dynamics (FMD),(*19*) wave packet molecular dynamics (WPMD),(*20*) and floating spherical Gaussian orbital (FSGO) methods.(*21*) In eFF, the electrons $\{j\}$ are represented by floating spherical Gaussian (FSG) wave packets with the Cartesian coordinates of the center of the FSG $\overrightarrow{R_j}$ and the FSG width (size) s_j as variables. The total wavefunction is a Hartree product of single-electron wave packets:

$$\Psi(\overrightarrow{r_i}) \propto \prod_j \exp\left[-\left(\frac{1}{s_j^2} - \frac{2p_{s_j}}{s_j}\frac{i}{\hbar}\right)\left(\overrightarrow{r_j} - \overrightarrow{R_j}\right)^2\right] \exp\left[\frac{i}{\hbar}\overrightarrow{p}_{\overrightarrow{R_j}} \cdot \overrightarrow{r_j}\right]. \qquad (5.1)$$

The normalized wavefunction of each electron is

$$\phi_j(\overrightarrow{r_j}) = \left(\frac{\sqrt{2}}{\sqrt{\pi}s_j}\right)^{\frac{3}{2}} \exp\left[-\frac{(\overrightarrow{r_j} - \overrightarrow{R_j})^2}{s_j^2}\right]. \qquad (5.2)$$

The use of Hartree product instead of antisymmetric wavefunctions reduces the $O(N^4)$ scaling of pairwise electrostatic energy evaluations to $O(N^2)$, which is

desirable. To account for the energy contribution from antisymmetrization, we include a Pauli potential in the total energy expression. The total energy E is thus the sum of Hartree product electronic kinetic energy E_{ke}, Hartree product electrostatic energies $E_{\text{nuc-nuc}}$, $E_{\text{nuc-elec}}$, $E_{\text{elec-elec}}$, and Pauli energy E_{Pauli}:

$$E = E_{\text{ke}} + E_{\text{nuc-nuc}} + E_{\text{nuc-elec}} + E_{\text{elec-elec}} + E_{\text{Pauli}}, \tag{5.3}$$

where

$$\begin{aligned}
E_{\text{ke}} &= \sum_j \langle j| -\frac{1}{2}\nabla_j^2 |j\rangle = \sum_j \frac{3}{2}\frac{1}{s_j^2} \\
E_{\text{nuc-nuc}} &= \sum_{m<n} \frac{Z_m Z_n}{R_{mn}} = \sum_{m<n} \frac{Z_m Z_n}{R_{mn}} \\
E_{\text{nuc-elec}} &= \sum_{n,j} \langle j| -\frac{Z_n}{r_{nj}} |j\rangle = -\sum_{n,j} \frac{Z_n}{R_{nj}} \text{Erf}\left(\frac{\sqrt{2}R_{nj}}{s_j}\right) \\
E_{\text{elec-elec}} &= \sum_{i<j} \langle ij| \frac{1}{r_{ij}} |ij\rangle = \sum_{i<j} \frac{1}{R_{ij}} \text{Erf}\left(\frac{\sqrt{2}R_{ij}}{\sqrt{s_i^2 + s_j^2}}\right) \\
E_{\text{Pauli}} &= \sum_{\sigma_i=\sigma_j} E(\uparrow\uparrow)_{ij} + \sum_{\sigma_i\neq\sigma_j} E(\uparrow\downarrow)_{ij}
\end{aligned} \tag{5.4}$$

in which Z_n represents the charge of the nucleus n, σ_j represents the spin of electron j, and

$$\begin{aligned}
E(\uparrow\uparrow)_{ij} &= \left(\frac{\bar{S}_{ij}^2}{1-\bar{S}_{ij}^2} + (1-\rho)\frac{\bar{S}_{ij}^2}{1+\bar{S}_{ij}^2}\right)\Delta\bar{T}_{ij} \\
E(\uparrow\downarrow)_{ij} &= \frac{\rho\bar{S}_{ij}^2}{1+\bar{S}_{ij}^2}\Delta\bar{T}_{ij},
\end{aligned} \tag{5.5}$$

where $\rho = -0.2$.

The overlap integral of electrons i and j is

$$S_{ij} = \langle i|j\rangle = \left(\frac{2s_i s_j}{s_i^2 + s_j^2}\right)^{3/2} \exp\left(-\frac{R_{ij}^2}{s_i^2 + s_j^2}\right), \tag{5.6}$$

and the change of electronic kinetic energy upon antisymmetrization of the wave-

function is

$$\begin{aligned}\Delta T_{ij} &= \langle\Psi_{\text{Slater}}|-\frac{1}{2}\nabla_i^2-\frac{1}{2}\nabla_j^2|\Psi_{\text{Slater}}\rangle-\langle\Psi_{\text{Hatree}}|-\frac{1}{2}\nabla_i^2-\frac{1}{2}\nabla_j^2|\Psi_{\text{Hartree}}\rangle \\ &= \frac{S_{ij}^2}{1-S_{ij}^2}(t_{ii}+t_{jj}-2t_{ij}/S_{ij}) \\ &= \frac{S_{ij}^2}{1-S_{ij}^2}\left[\frac{3}{2}\frac{1}{s_i^2}+\frac{3}{2}\frac{1}{s_j^2}-\frac{6}{s_i^2+s_j^2}+\frac{4R_{ij}^2}{(s_i^2+s_j^2)^2}\right], \end{aligned} \tag{5.7}$$

where

$$\Psi_{\text{Slater}} = \frac{1}{\sqrt{2-2S_{ij}^2}}(\phi_i\phi_j-\phi_j\phi_i) \tag{5.8}$$

$$\Psi_{\text{Hartree}} = \phi_i\phi_j. \tag{5.9}$$

While S_{ij} and ΔT_{ij} are functions of s_i and R_{ij}, we define $\bar{S}_{ij}$ and $\Delta\bar{T}_{ij}$ as functions of $\bar{s}_i = a_s s_i$ and $\bar{R}_{ij} = a_R R_{ij}$, where $a_s = 0.9$ and $a_R = 1.125$. The parameters ρ, a_s, a_R are universal parameters that were adjusted to reproduce the geometries for a range of structures.(*22*)

By substituting the wave packet into the time-dependent Schrödinger equation, one could derive the Hamilton equation of motion:

$$\begin{aligned}\dot{\overrightarrow{p}}_{\overrightarrow{R_j}} &= -\nabla_{\overrightarrow{R_j}}E,\ \dot{p}_{s_j} = -\frac{\partial E}{\partial s_j} \\ \overrightarrow{p}_{\overrightarrow{R_j}} &= m_{elec}\dot{\overrightarrow{R_j}},\ p_{s_j} = \frac{3m_e}{4}\dot{s_j}, \end{aligned} \tag{5.10}$$

where m_e is the mass of the electron. The nuclear motion is governed by

$$\dot{\overrightarrow{p}}_{\overrightarrow{R_n}} = -\nabla_{\overrightarrow{R_n}}E, \tag{5.11}$$

$$\overrightarrow{p}_{\overrightarrow{R_n}} = m_n\dot{\overrightarrow{R_n}}, \tag{5.12}$$

where m_n is the mass of the nucleus.

This equation of motion shows the average position of the wave packet follows a classical trajectory, consistent with Ehrenfest's theorem. It extends the Ehrenfest's theorem in that the size of the wave packet also follows a classical trajectory.

The above summarizes the eFF formulation. Two assumptions were made to develop the Pauli potential in Equation 5.5: 1) the Pauli energy can be approximated

by the sum of pair-wise interaction energies of elections, and 2) the kinetic energy component dominates the energy change caused by antisymmetrization of the wavefunction (the Pauli energy). The functional form comes from mixing

$$E_u = \langle \Psi_{\text{Slater}}| -\frac{1}{2}\nabla_i^2 - \frac{1}{2}\nabla_j^2 |\Psi_{\text{Slater}}\rangle - \langle \Psi_{\text{Hatree}}| -\frac{1}{2}\nabla_i^2 - \frac{1}{2}\nabla_j^2 |\Psi_{\text{Hartree}}\rangle$$

and a correlation energy

$$E_g = \langle \Psi_{\text{VB}}| -\frac{1}{2}\nabla_i^2 - \frac{1}{2}\nabla_j^2 |\Psi_{\text{VB}}\rangle - \langle \Psi_{\text{Hatree}}| -\frac{1}{2}\nabla_i^2 - \frac{1}{2}\nabla_j^2 |\Psi_{\text{Hartree}}\rangle,$$

where

$$\Psi_{\text{VB}} = \frac{1}{\sqrt{2+2S_{ij}^2}}(\phi_i\phi_j + \phi_j\phi_i). \tag{5.13}$$

Klakow (*23*) used $E(\uparrow\uparrow) = E_u$ and $E(\uparrow\downarrow) = 0$ in kinetic-energy-based Pauli potentials. To reduce the likelihood of coalescence for both same spin and opposite spin electrons, eFF chose

$$\begin{aligned} E(\uparrow\uparrow) &= E_u - (1-\rho)E_g \\ E(\uparrow\downarrow) &= -\rho E_g. \end{aligned} \tag{5.14}$$

This is discussed in detail in (*22*) by Su.

5.3 The Gaussion Hartree Approximated Quantum Mechanics Framework

Recently, Xiao (*18*) questioned the justification of the above two assumptions in eFF Pauli potential. This led to the early development of the GHA-QM formulation of the Pauli potential in 2014. He suggested that the electron-electron and electron-nucleus Coulomb components of the energy change upon antisymmetrization are not negligible. Also, the Pauli potential considering only pair-wise interactions does not scale correctly with the number of electrons, and a scaling factor is introduced.

The total energy change upon antisymmetrization in GHA-QM is written as

$$E_{\text{Pauli}} = \sum_{\sigma_i=\sigma_j} F(\uparrow\uparrow)_{ij} E_{\text{Pauli}}^{\text{base}}(\uparrow\uparrow)_{ij} + \sum_{\sigma_i\neq\sigma_j} F(\uparrow\downarrow)_{ij} E_{\text{Pauli}}^{\text{base}}(\uparrow\downarrow)_{ij}, \tag{5.15}$$

where $F(\uparrow\uparrow)_{ij}$ and $F(\uparrow\downarrow)_{ij}$ are the scaling factors,

$$E_{\text{Pauli}}^{\text{base}}(\uparrow\uparrow)_{ij} = \Delta T_{ij} + \Delta C_{ee,i,j} + \sum_n \Delta C_{ne,i,j} \tag{5.16}$$

and

$$E_{\text{Pauli}}^{\text{base}}(\uparrow\downarrow)_{ij} = -\frac{p_0 S_{ij}^{p_1} + p_2 S_{ij}^{p_3} \bar{s}_{ij}^{p_4}}{1 + p_5 S_{ij}^{p_6} + p_7 S_{ij}^{p_8} \bar{s}_{ij}^{p_9}} \tag{5.17}$$

in which ΔT_{ij} is defined the same as Equation 5.7, S_{ij} is defined the same as Equation 5.6, and

$$\bar{s}_{ij} = \frac{s_i s_j}{\sqrt{s_i^2 + s_j^2}}. \tag{5.18}$$

$E^{\text{base}}_{\text{Pauli}}(\uparrow\downarrow)_{ij}$ accounts for electron correlation and the form is inspired by the Wigner correlation functional, and $p_k,\ k = 0, ...9$ are parameters fitted to singlet H_2 bonding curve calculated using B3LYP/FSG.

$\Delta C_{ee,ij}$ and $\Delta C_{ne,ij}$ come from the electron-electron and electron-nucleus Coulomb terms in the total Hamiltonian of an electron pair

$$\hat{H} = -\sum_{k=1,2}\frac{1}{2}\nabla_k^2 + \frac{1}{r_{12}} - \sum_n \sum_{k=1,2}\frac{Z_n}{r_{nk}}. \tag{5.19}$$

Similar to the derivation of ΔT_{12} in Equation 5.7,

$$\begin{aligned}\Delta C_{ee,12} &= \langle\Psi_{\text{Slater}}|\frac{1}{r_{12}}|\Psi_{\text{Slater}}\rangle - \langle\Psi_{\text{Hatree}}|\frac{1}{r_{12}}|\Psi_{\text{Hartree}}\rangle \\ &= O_{12}(J_{12} - K_{12}/S_{12}^2),\end{aligned} \tag{5.20}$$

where

$$O_{12} = \frac{S_{12}^2}{1 - S_{12}^2}, \tag{5.21}$$

$$J_{12} = \langle 12|\frac{1}{r_{12}}|12\rangle = \frac{1}{R_{12}}\text{Erf}\left(\frac{\sqrt{2}R_{12}}{\sqrt{s_1^2 + s_2^2}}\right), \tag{5.22}$$

and the exchange energy

$$K_{12} = \langle 12|\frac{1}{r_{12}}|21\rangle = \sqrt{\frac{2}{\pi}}\frac{\sqrt{s_1^2 + s_2^2}}{s_1 s_2}S_{12}^2. \tag{5.23}$$

For the nucleus-electron Coulomb interaction contribution,

$$\begin{aligned}\Delta C_{ne,12} &= \langle\Psi_{\text{Slater}}| - \frac{Z_n}{r_{n1}} - \frac{Z_n}{r_{n2}}|\Psi_{\text{Slater}}\rangle - \langle\Psi_{\text{Hatree}}| - \frac{Z_n}{r_{n1}} - \frac{Z_n}{r_{n2}}|\Psi_{\text{Hartree}}\rangle \\ &= O_{12}(j_{11} + j_{22} - 2j_{12}/S_{12}^2),\end{aligned} \tag{5.24}$$

where

$$j_{kk} = \langle k| - \frac{Z_n}{r_{nk}}|k\rangle = -Z_n\frac{\text{Erf}\left(\frac{\sqrt{2}}{s_k}R_{nk}\right)}{R_{nk}} \quad (k = 1, 2) \tag{5.25}$$

$$j_{12} = \langle 1| - \frac{Z_n}{r_{n1}}|2\rangle = -\frac{Z_n}{\bar{s}_{12}} \frac{\mathrm{Erf}\left(\sqrt{\frac{R_{n1}^2}{s_1^2} + \frac{R_{n2}^2}{s_2^2} - \frac{R_{12}^2}{s_1^2+s_2^2}}\right)}{\sqrt{\frac{R_{n1}^2}{s_1^2} + \frac{R_{n2}^2}{s_2^2} - \frac{R_{12}^2}{s_1^2+s_2^2}}} S_{12}. \tag{5.26}$$

The full forms of the scaling factors in Equation 5.15 are

$$F(\uparrow\uparrow)_{ij} = F(\uparrow\uparrow)_{ij,\mathrm{sym}}(\Delta T, \Delta C_{ee}, \Delta C_{ne}) F(\uparrow\uparrow)_{ij,\mathrm{asym}}(\Delta T, \Delta C_{ee}, \Delta C_{ne}) \tag{5.27}$$

and

$$F(\uparrow\downarrow)_{ij} = F(\uparrow\downarrow)_{ij,\mathrm{sym}} F(\uparrow\downarrow)_{ij,\mathrm{asym}}. \tag{5.28}$$

Define

$$\overline{\sum} S_{ij} = \frac{1}{2}\left(\sum_k S_{ik} + \sum_{k'} S_{ik'}\right) \tag{5.29}$$

$$\overline{\sum} S_{ij}^2 = \frac{1}{2}\left(\sum_k S_{ik}^2 + \sum_{k'} S_{ik'}^2\right). \tag{5.30}$$

For same spin electrons that each has exactly the same environment, the scaling factors for ΔT and ΔC_{ne} can be derived based on D_{3h} quartet H_3 or T_d quintet H_4 to give

$$F(\uparrow\uparrow)_{ij,\mathrm{sym}}(\Delta T, \Delta C_{ne}) = \frac{1 + S_{ij}}{1 + \overline{\sum} S}. \tag{5.31}$$

Therefore, we separate the scaling factor into two terms multiplying each other, F_{sym} and F_{asym}, which account for the "symmetric" environment and "asymmetric" environment, respectively.

The forms of the other components of the same spin electron scaling factors are

$$\begin{aligned} F(\uparrow\uparrow)_{ij,\mathrm{sym}}(\Delta C_{ee}) = {} & p_{se0}\left(\frac{p_{se1} + S_{ij}}{p_{se1} + \overline{\sum} S_{ij}} + \frac{\overline{\sum} S_{ij} - S_{ij}}{p_{se1} S_{ij} + \overline{\sum} S_{ij}}\right)^{p_{se2}} \\ & + (1 - p_{se0})\left(\frac{p_{se3} + S_{ij}^2}{p_{se3} + \overline{\sum} S_{ij}^2} + \frac{\overline{\sum} S_{ij}^2 - S_{ij}^2}{p_{se3} S_{ij}^2 + \overline{\sum} S_{ij}^2}\right)^{p_{se4}}, \end{aligned} \tag{5.32}$$

where the parameters $p_{sek}, k = 0, ..., 4$ are fitted with the exact quantum mechanics [unrestricted Hartree Fock (UHF)/FSG] results of D_{3h} quartet H_3 and T_d quintet H_4 symmetric stretching, and

$$\begin{aligned} F(\uparrow\uparrow)_{ij,\mathrm{asym}}(\Delta T, \Delta C_{ee}, \Delta C_{ne}) = {} & 1 + p_{a0}\left(S_{ij}\overline{\sum} S_{ij} - \overline{\sum} S_{ij}^2\right) \\ & + p_{a1}\left(S_{ij}\overline{\sum} S_{ij} - \overline{\sum} S_{ij}^2\right)^2 \\ & + p_{a2}\left(S_{ij}\overline{\sum} S_{ij} - \overline{\sum} S_{ij}^2\right)^3, \end{aligned} \tag{5.33}$$

where $p_{ak}, k = 0, 1, 2$ are parameters whose values depend on whether it is for ΔT, ΔC_{ee} or ΔC_{ne}, and fitted with D_{3h} to C_{2v} transition of quartet H_3 and T_d to C_{3v} transition of quintet H_4.

For opposite spin scaling factors, the forms are

$$F(\uparrow\downarrow)_{ij,\mathrm{sym}} = p_{os0}\left(\frac{1+p_{os1}S_{ij}}{1+p_{os1}\overline{\sum}S_{ij}}\right)^{p_{os2}} + (1-p_{os0})\left(\frac{1+p_{os3}S_{ij}^2}{1+p_{os3}\overline{\sum}S_{ij}^2}\right)^{p_{os4}}, \quad (5.34)$$

where the parameters $p_{osk}, k = 0, ..., 4$ are fitted with $D_{\infty h}$ doublet H_3 and D_{4h} singlet H_4 symmetric stretching, and

$$\begin{aligned} F(\uparrow\downarrow)_{ij,\mathrm{asym}} &= 1 + p_{oa0}\left(\frac{S_{ij}\overline{\sum}S_{ij} - \overline{\sum}S_{ij}^2}{S_{ij}\overline{\sum}S_{ij} + \overline{\sum}S_{ij}^2}\right) \\ &\quad + p_{oa1}\left(\frac{S_{ij}\overline{\sum}S_{ij} - \overline{\sum}S_{ij}^2}{S_{ij}\overline{\sum}S_{ij} + \overline{\sum}S_{ij}^2}\right)^2 \\ &\quad + p_{oa2}\left(\frac{S_{ij}\overline{\sum}S_{ij} - \overline{\sum}S_{ij}^2}{S_{ij}\overline{\sum}S_{ij} + \overline{\sum}S_{ij}^2}\right)^3, \end{aligned} \quad (5.35)$$

where the parameters $p_{oak}, k = 0, 1, 2$ are fitted with $D_{\infty h}$ doublet H_3 and D_{4h} singlet H_4 asymmetric stretching.

In summary, the total Pauli potential for same spin electron pairs is

$$\begin{aligned} E_{\mathrm{Pauli}}(\uparrow\uparrow)_{ij} &= F(\uparrow\uparrow)_{ij,\mathrm{sym}}(\Delta T)F(\uparrow\uparrow)_{ij,\mathrm{asym}}(\Delta T)\Delta T_{ij} \\ &\quad + F(\uparrow\uparrow)_{ij,\mathrm{sym}}(\Delta C_{ee})F(\uparrow\uparrow)_{ij,\mathrm{asym}}(\Delta C_{ee})\Delta C_{ee,ij} \\ &\quad + \sum_n F(\uparrow\uparrow)_{ij,\mathrm{sym}}(\Delta C_{ne})F(\uparrow\uparrow)_{ij,\mathrm{asym}}(\Delta C_{ne})\Delta C_{ne,ij} \end{aligned} \quad (5.36)$$

and the total Pauli potential for opposite spin pairs is

$$E_{\mathrm{Pauli}}(\uparrow\downarrow)_{ij} = F(\uparrow\downarrow)_{ij,\mathrm{sym}}F(\uparrow\downarrow)_{ij,\mathrm{asym}}E^{\mathrm{base}}_{\mathrm{Pauli}}(\uparrow\downarrow)_{ij}. \quad (5.37)$$

The above has been discussed in more detail in (*18*).

5.4 Improvements on GHA-QM

The GHA-QM framework in the previous section produces QM quality bonding curve for singlet and triplet H_2, and gives good results for symmetric and asymmetric stretching of H_3 and H_4 molecules in mild conditions. However, when we tested the system more substantially and tried to simulate hydrogen systems with more electrons in high density, we found certain problems. This section discusses several strategies that were taken to fix these problems.

New Opposite Spin Pauli Potential

We found that the size of the electron in the center of linear H_3 sometimes goes to zero. This is because in Equation 5.17 where p_4 is negative and all other parameters are positive, one electron having zero size ($\bar{s}$ going to zero) means $E^{\text{base}}_{\text{Pauli}}(\uparrow\downarrow)$ becomes negative infinite and energetically favored. To avoid this problem, we introduced a positive shift p_{10} of electron size in Equation 5.17. The new form is

$$E^{\text{base}}_{\text{Pauli}}(\uparrow\downarrow)_{ij} = -\frac{p_0 S_{ij}^{p_1} + p_2 S_{ij}^{p_3} (\bar{s}_{ij} + p_{10})^{p_4}}{1 + p_5 S_{ij}^{p_6} + p_7 S_{ij}^{p_8} \bar{s}_{ij}^{p_9}}. \tag{5.38}$$

We refitted the parameters against the exact QM results of singlet H_2 bonding curve.(*24*) The new parameters are $p_0 = 0.439387, p_1 = 2.914263, p_2 = 8.180823, p_3 = 6.100496, p_4 = -18.088005, p_5 = 0.698750, p_6 = 3.305666, p_7 = 2.031224, p_8 = 7.359878, p_9 = 5.552337, p_{10} = 8.345865$. The resulting GHA-QM H_2 bonding curve is nearly exact in the bonding regions, and performs better than B3LYP/6-311++G** at intermediate bond lengths (Figure 5.1). Because the base energy of the

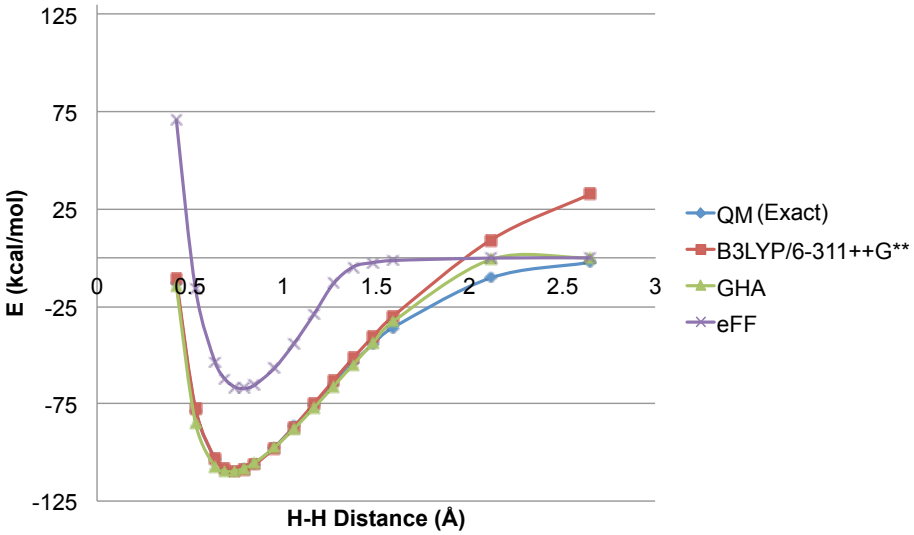

Figure 5.1: Performance of GHA-QM on single H_2.

opposite spin Pauli potential has changed, we refitted the parameters in the opposite spin scaling factors too. We used genetic algorithm to train the parameters for both symmetric and asymmetric scaling factors at the same time. The best parameters are $p_{os0} = 0.968658, p_{os1} = 1.021811, p_{os2} = 2.720616, p_{os3} = 15.859202, p_{os4} = 20.201212$ and $p_{oa0} = 2.376509, p_{oa1} = 18.590298, p_{oa2} = 13.245066$. These parameters give much improved energy for H_3 reaction path (Figure 5.2), and overall

a more accurate H_3 potential energy surface (Figure 5.4) than eFF (Figure 5.5) comparing to *ab initio* H_3 potential energy surface (Figure 5.5).(*25*)

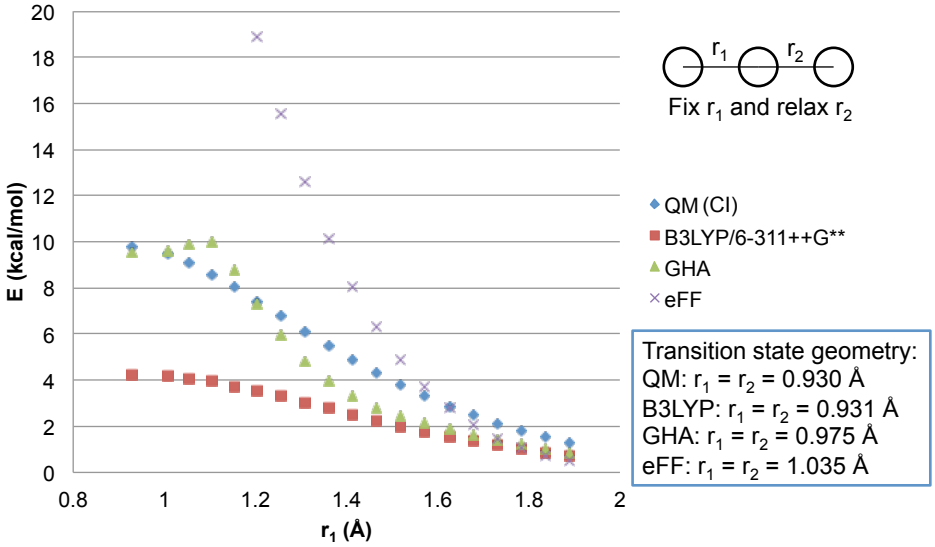

Figure 5.2: Performance of GHA-QM on H_3 reaction path. The QM configuration interaction (CI) data is from (*26*).

Preventing Same Spin Electron Coalescence

When we tried to simulate the equation of state (EOS) of a dense H_2 liquid (Wigner radius $r_s = 2.2$ bohr), we find the same spin electrons are energetically favorable to diffuse and cluster at some configurations. The following paragraphs are devoted to attempts at solving this problem.

A New Form of ΔT We'd like to shift the numerator in Equation 5.7 by a small amount dd so that ΔT goes to infinity when $S \to 1$. For convenience, the subscripts of $\Delta T, S, O$ are omitted.

The new form is

$$\begin{aligned} \Delta T &= \frac{S^2(t_{11} + t_{22} - 2t_{12}/S) + dd}{1 - S^2} \\ &= \frac{S^2\left[\frac{3}{2}\frac{1}{s_1^2} + \frac{3}{2}\frac{1}{s_2^2} - \frac{6}{s_1^2+s_2^2} + \frac{4R_{12}^2}{(s_1^2+s_2^2)^2}\right] + dd}{1 - S^2} \\ &= O \cdot T + \frac{dd}{1 - S^2}, \end{aligned} \tag{5.39}$$

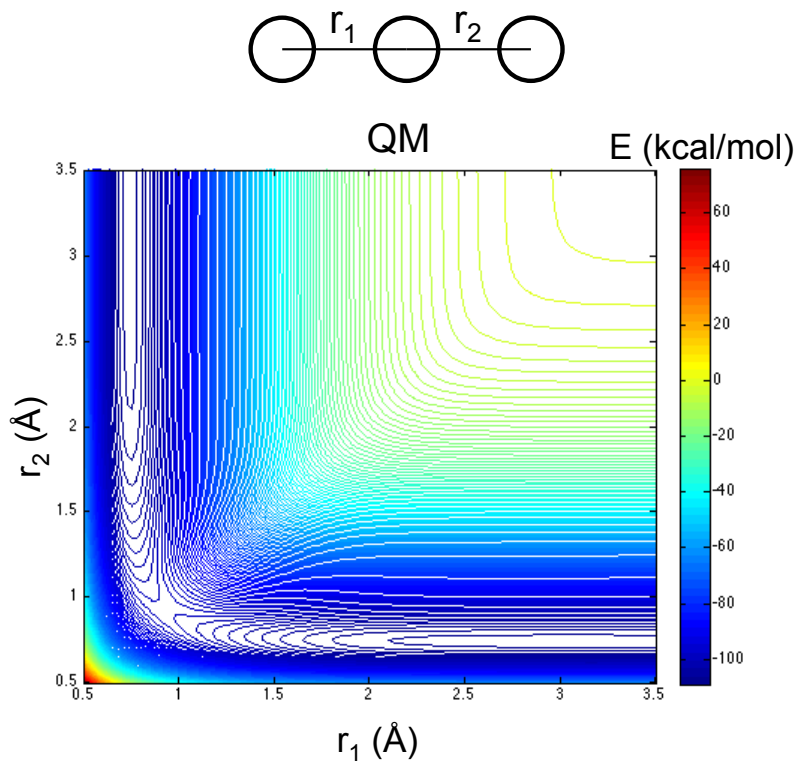

Figure 5.3: Analytical H_3 potential energy surface. The data is from (*25*).

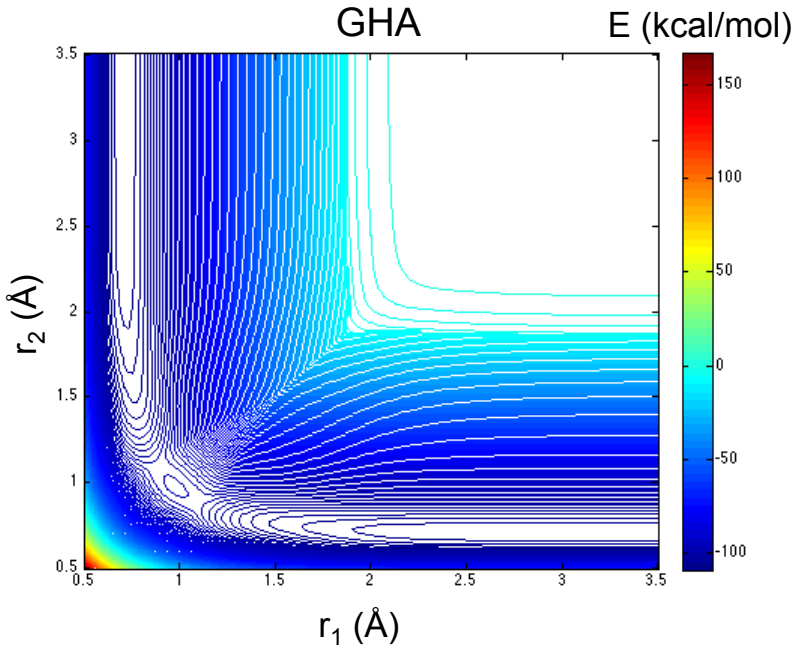

Figure 5.4: GHA-QM H_3 potential energy surface. r_1 and r_2 are defined in Figure 5.3.

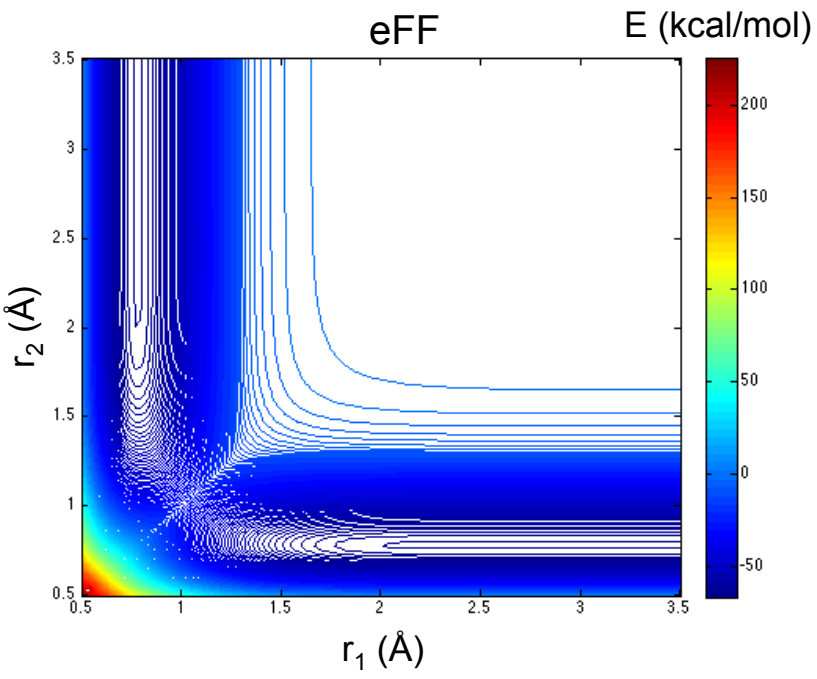

Figure 5.5: eFF H_3 potential energy surface. r_1 and r_2 are defined in Figure 5.3.

where

$$T \equiv \frac{3}{2}\frac{1}{s_1^2} + \frac{3}{2}\frac{1}{s_2^2} - \frac{6}{s_1^2 + s_2^2} + \frac{4R_{12}^2}{(s_1^2 + s_2^2)^2}.$$

We chose $dd = 1.0 \times 10^{-4}$.

To avoid numerical instability when $S \to 1$, $s_1 \to s_2$ and $R_{12} \to 0$, we did series expansion of ΔT at this condition (Appendix D). In its practical implementation, when $1 - S^2 \leq 0.001$, instead of the form in Equation 5.39, we take

$$\Delta T = \left(\frac{1}{s_1 s_2} - \frac{R_{12}^2}{2s_1^2 s_2^2} + \frac{R_{12}^4}{12 s_1^3 s_2^3}\right) + dd\left(\frac{s_1 s_2}{R_{12}^2} + \frac{1}{2} + \frac{R_{12}^2}{12 s_1 s_2} - \frac{R_{12}^6}{720 s_1^3 s_2^3}\right). \quad (5.40)$$

Although this scheme can prevent the same spin electrons to have the same coordinates, it does not prevent same spin electrons of similar sizes to become unphysically close (overlap $S \to 1$). As can be seen in Figure 5.6, the energy penalty from the new form of ΔT is not big enough for most configurations the dynamics simulation can reach. Nevertheless, we kept this form because it does prevent the same spin electrons to have the same coordinates and enforce the Pauli exclusion principle.

New Same Spin Scaling Factors The form of Equation 5.33 may cause serious issues during simulation because it is unbounded. In addition, the sign of the

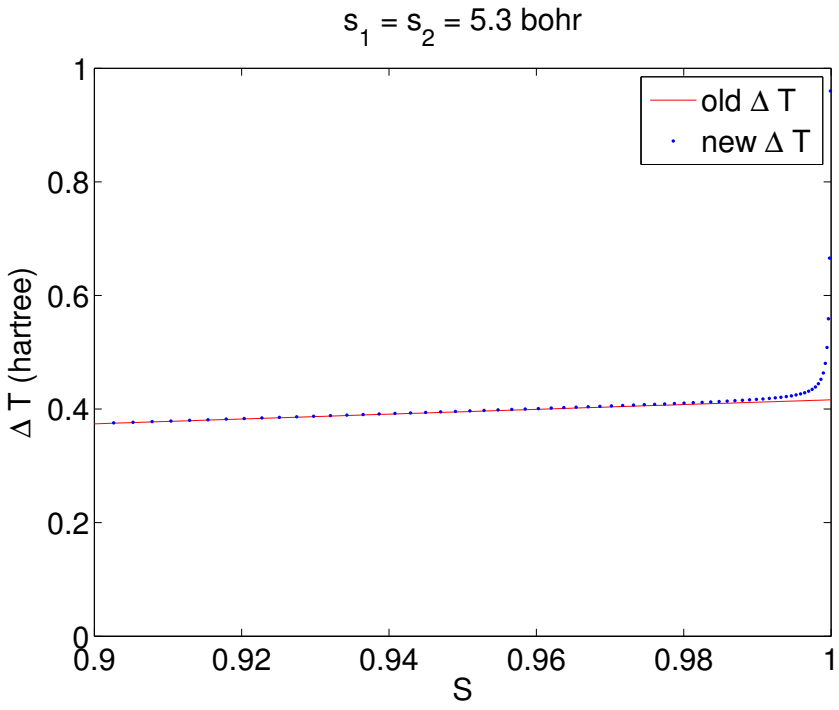

Figure 5.6: Comparison of ΔT values from the old and new forms for diffused electrons of the same size and spin.

function may change due to the odd powers and the possibility for $(S_{ij}\overline{\sum}S_{ij} - \overline{\sum}S_{ij}^2)$ to become negative in some cases. To make the function bounded, we adopt the following form instead:

$$F(\uparrow\uparrow)_{ij,\text{asym}}(\Delta T, \Delta C_{ee}, \Delta C_{ne}) = 1 + p_{a0}D_{ij} + p_{a1}D_{ij}^2 + p_{a2}D_{ij}^3, \tag{5.41}$$

where $D_{ij} = \left(\frac{S_{ij}\overline{\sum}S_{ij} - \overline{\sum}S_{ij}^2}{S_{ij}\overline{\sum}S_{ij} + \overline{\sum}S_{ij}^2 + d}\right)$. The small constant $d = 1.0 \times 10^{-6}$ is to prevent the denominator from going to zero when all the overlap $S \to 0$. In fact, this shift has been added to the opposite spin asymmetric scaling factor too so that now same spin and opposite spin asymmetric scaling factors adopt the same form, with different parameters. The parameters for same spin asymmetric scaling factors are summarized in Table 5.1.

For the fitting to cover the whole range of S values from 0 to 1, we fitted against C_{2v} quartet H_3, with one H-H distance fixed at 0.1 bohr and 1.7 bohr. The size of the electrons were kept to 1.5 bohr. Figures 5.7 shows that the whole range of S has been covered, especially for large S values that were not considered in previous fitting.

	ΔT	ΔC_{ee}	ΔC_{ne}
p_{a0}	1.31546298328185	0.727335080043498	0.468486643682531
p_{a1}	3.39853157886649	1.311794439120800	13.20277753109270
p_{a2}	2.33306859558464	0.584459359077299	12.98429088741020

Table 5.1: New parameters for same spin asymmetric scaling factors $F(\uparrow\uparrow)_{ij,\text{asym}}(\Delta T, \Delta C_{ee}, \Delta C_{ne})$.

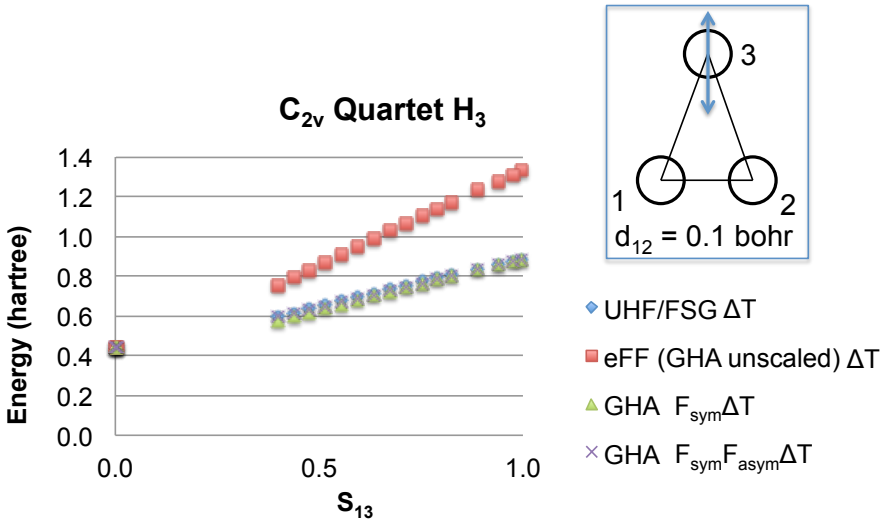

Figure 5.7: Performance of GHA-QM for C_{2v} quartet H_3 with one H-H distance fixed at 0.1 bohr.

Figure 5.8 shows the GHA-QM same spin symmetric scaling factor does not work for C_{2v} quartet H_3 when one H-H distance is fixed at 1.7 bohr and the other H-H distances are much smaller than 1.7 bohr. This suggests that the symmetric scaling factor is not likely able to deal with linear H_3. Since the same spin symmetric scaling factor for ΔT is exact for D_{3h} H_3, we hypothesized that the scaling factors are highly symmetry-dependent and the $F(\uparrow\uparrow)_{\text{sym}}$ derived from D_{3h} H_3 cannot be universally applied to all molecules with other symmetry. Interestingly, eFF seems to go to the correct limit as the system approaches being linear. To further explore this issue, we developed a scaling factor $F(\uparrow\uparrow)_{\text{linear}}$ to replace $F(\uparrow\uparrow)_{\text{sym}}$ in linear molecules:

$$F(\uparrow\uparrow)_{ij,\text{linear}} = 1 + p_{l0}v + p_{l1}v^2 + p_{l2}v^3, \tag{5.42}$$

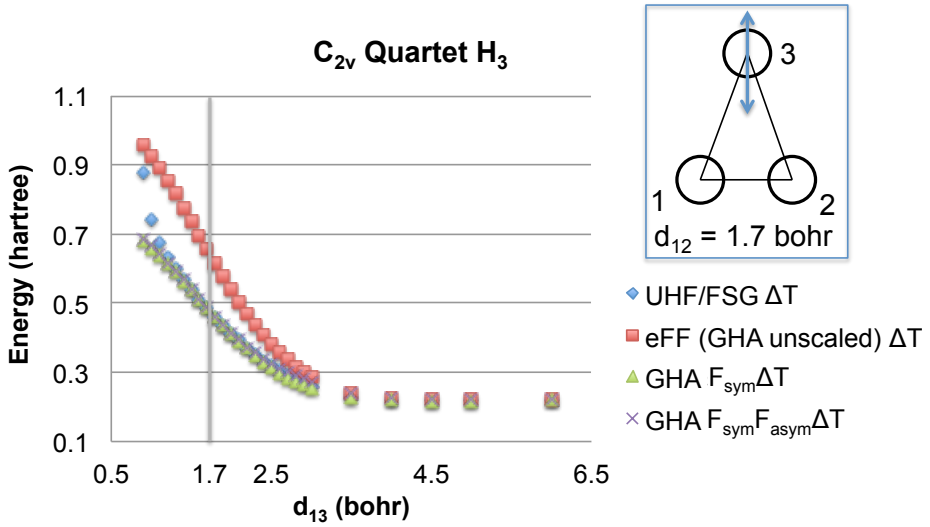

Figure 5.8: Performance of GHA-QM for C_{2v} quartet H_3 with one H-H distance fixed at 1.7 bohr.

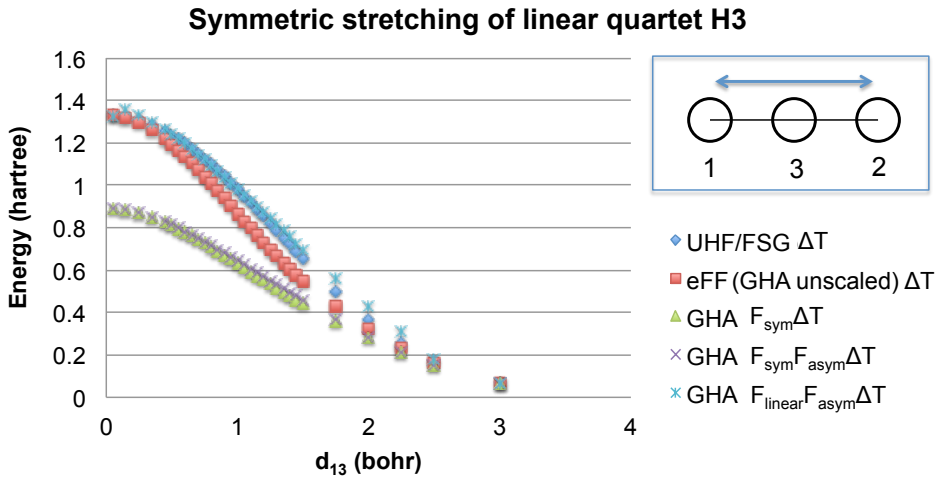

Figure 5.9: Comparison of the effect of different scaling factors in the performance of symmetric stretching of linear quartet H_3.

where

$$v = \left(\frac{(S_{ij} \sum S_{ij} - \sum S_{ij}^2)^2}{(p_{l3} S_{ij} \sum S_{ij} - \sum S_{ij}^2)^2 + d_l} \right), \tag{5.43}$$

we chose $d_l = 1.0 \times 10^{-7}$ and fitted the parameters $p_{l0} = 0.0098195829828946$, $p_{l1} = 0.0758036465880992$, $p_{l2} = 0.440549994711866$, $p_{l3} = 0.999965221776706$.

Intuitively, when the H-H distances become very small, linear H_3 and D_{3h} H_3 energy should go to the same limit. However, this is not the case as seen from Figure 5.9.

This confirms that the scaling factors should be symmetry-dependent or geometry-dependent. However, in practice it is likely impossible to implement. Since our goal is to simulate condensed matters, there will be too many electrons in the system for the program to classify the configuration to determine suitable scaling factors.

Removing the Same Spin Scaling Factors The analysis in the previous subsection suggests it might be a good idea to remove the same spin scaling factors completely (i.e. make them take the value of 1). In addition, minimization of the dense H_2 liquid ($r_s = 1.76$ bohr or denser) shows that same spin scaling factors for ΔT and ΔC_{ne} can scale these positive energy contributions down to $\sim \frac{1}{10}$ times the base values while maintaining the negative energy contribution from ΔC_{ee} similar to the base value. This energetically favors the same spin electrons to cluster, even when we keep the electron sizes fixed at 1.55 bohr (the electron size in H_2 optimized by GHA-QM). The different behaviors of the scaling factors for different energy components may be due to the empirical nature of some of the functional forms of the scaling factors, and may also be due to the symmetry issue discussed in the previous subsection.

To see how much removing same spin scaling factors could affect molecular interactions, we calculated the H_2-H_2 association curve with GHA-QM without same spin scaling factors. The results look reasonable as they are close to QM results (*27*) in Figure 5.10. They are also an improvement on eFF.

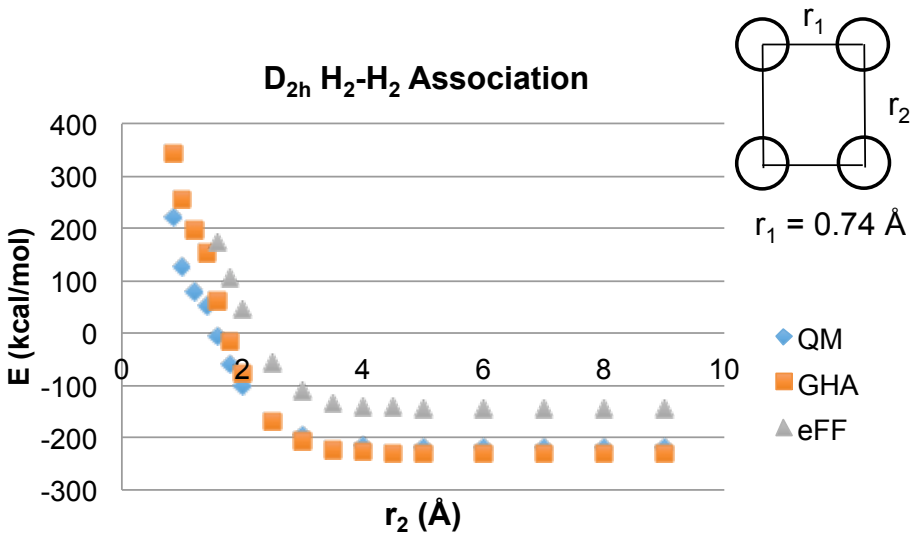

Figure 5.10: D_{2h} H_2-H_2 association without same spin scaling factors. The energy values are $E(H_4) - 4E(H)$. The QM data is from (*27*).

Therefore, with the same spin scaling factors turned off, we went on to calculate the liquid H_2 EOS and compared it to QM results. A cubic box of 108 H_2 molecules has been used with minimum image on each side of the box as the periodic boundary condition. We took $m_e = m_H$ so that we can use a relatively large time step 0.02 femtosecond. A total of 2 ps dynamics was carried out for each temperature, and the first 0.5 ps was discarded when calculating the average pressure. During the dynamics, for each time step we optimized the electron sizes based on the x, y, z coordinates of the electrons and nuclei. For simplicity, we approximated the optimization procedure by carrying out only the first step of the Newton-Raphson method and considering the second derivative of only the electronic kinetic energy. Figure 5.11 shows both GHA-QM and eFF are quite close to QM results, with both eFF and GHA-QM having a tendency to underestimate the pressure at low density. At high density, GHA-QM has a tendency to underestimate the pressure, while eFF tends to overestimate the pressure. In terms of the energy-volume relationship, GHA-QM is clearly an improvement upon eFF (Figure 5.12).

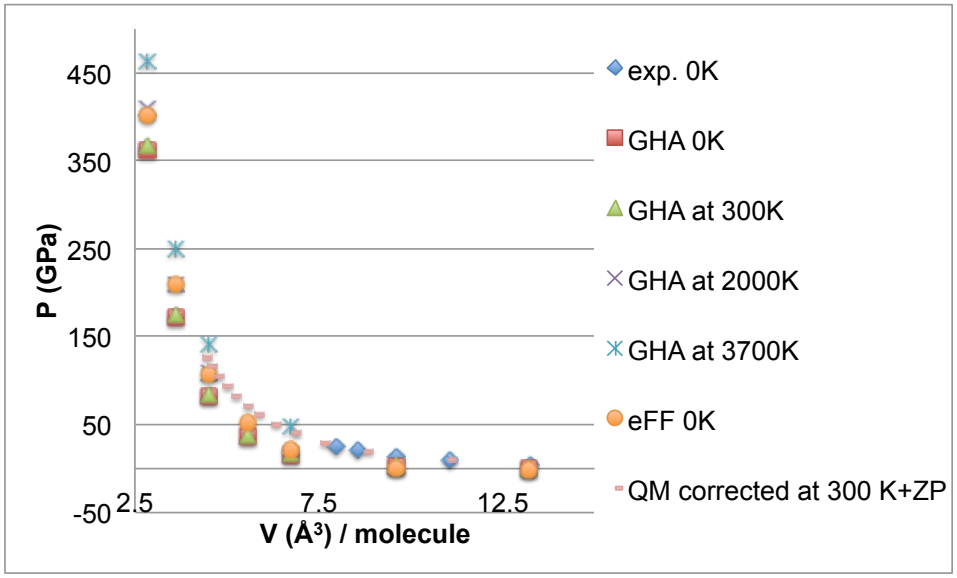

Figure 5.11: Pressure-volume diagram of H_2 liquid. The experimental values and QM extrapolation are from (*28*).

5.5 Conclusions and Future Work

We have overcome a few technical obstacles including but not limited to those discussed in the above section to enable large-scale simulations of warm dense hydrogen EOS using GHA-QM. Our next step is to simulate the shock hugoniot. We would like to see whether the new GHA-QM can correctly predict the pressure

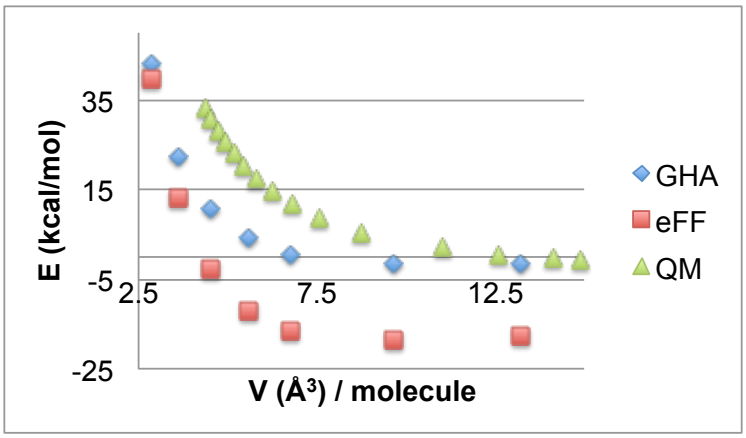

Figure 5.12: Energy-volume diagram of H_2 liquid. The QM data is generated by PBE-D3 calculation and provided by Saber Naserifar (unpublished).

and temperature where the hydrogen insulator-to-metal transition occurs. We may need to include the angular momentum projected effective core potential (AMPERE) extension,(*18*) which is not discussed here, to account for the cusp condition at the nuclei for more accurate predictions. When we move up in the periodic table, AMPERE will be necessary to obtain correct bond energy and nodal structures. In the future, we hope GHA-QM along with AMPERE will be able to simulate processes such as silicon etching that no existing method could simulate well.

References

(*1*) Landau, L., (1932). On the theory of transfer of energy at collisions II. *Phys. Z. Sowjetunion 2*, 7.

(*2*) Zener, C., In *Proceedings of the Royal Society of London A: Mathematical, Physical and Engineering Sciences*, 1932; Vol. 137, pp 696–702.

(*3*) McLachlan, A., (1964). A variational solution of the time-dependent Schrodinger equation. *Molecular Physics 8*, 39–44.

(*4*) Micha, D. A., (1983). A self-consistent eikonal treatment of electronic transitions in molecular collisions. *The Journal of Chemical Physics 78*, 7138–7145.

(*5*) Sawada, S.-I., Nitzan, A., and Metiu, H., (1985). Mean-trajectory approximation for charge-and energy-transfer processes at surfaces. *Physical Review B 32*, 851.

(*6*) Kirson, Z., Gerber, R., Nitzan, A., and Ratner, M. A., (1984). Dynamics of metal electron excitation in atom-surface collisions: A quantum wave packet approach. *Surface Science 137*, 527–550.

(*7*) Tully, J. C., and Preston, R. K., (1971). Trajectory surface hopping approach to nonadiabatic molecular collisions: the reaction of H+ with D2. *The Journal of Chemical Physics 55*, 562–572.

(*8*) Tully, J. C., (1990). Molecular dynamics with electronic transitions. *The Journal of Chemical Physics 93*, 1061–1071.

(*9*) Li, X., Tully, J. C., Schlegel, H. B., and Frisch, M. J., (2005). Ab initio Ehrenfest dynamics. *The Journal of chemical physics 123*, 084106.

(*10*) Isborn, C. M., Li, X., and Tully, J. C., (2007). Time-dependent density functional theory Ehrenfest dynamics: collisions between atomic oxygen and graphite clusters. *The Journal of chemical physics 126*, 134307–134307.

(*11*) Su, J. T., and Goddard III, W. A., (2007). Excited electron dynamics modeling of warm dense matter. *Physical review letters 99*, 185003.

(*12*) Takatsuka, K., Yonehara, T., Hanasaki, K., and Arasaki, Y., *Chemical Theory beyond the Born-Oppenheimer Paradigm: Nonadiabatic Electronic and Nuclear Dynamics in Chemical Reactions*; World Scientific: 2014.

(*13*) Kim, H., Su, J. T., and Goddard, W. A., (2011). High-temperature high-pressure phases of lithium from electron force field (eFF) quantum electron dynamics simulations. *Proceedings of the National Academy of Sciences 108*, 15101–15105.

(*14*) Theofanis, P. L., Jaramillo-Botero, A., Goddard III, W. A., Mattsson, T. R., and Thompson, A. P., (2012). Electron dynamics of shocked polyethylene crystal. *Physical Review B 85*, 094109.

(*15*) Su, J. T., and Goddard, W. A., (2009). Mechanisms of Auger-induced chemistry derived from wave packet dynamics. *Proceedings of the National Academy of Sciences 106*, 1001–1005.

(*16*) Chenard-Lemire, C., Lewis, L., and Meunier, M., (2012). Laser-induced Coulomb explosion in C and Si nanoclusters: The determining role of pulse duration. *Applied Surface Science 258*, 9404–9407.

(*17*) Theofanis, P. L., Jaramillo-Botero, A., Goddard III, W. A., and Xiao, H., (2012). Nonadiabatic study of dynamic electronic effects during brittle fracture of silicon. *Physical review letters 108*, 045501.

(*18*) Xiao, H., First principles based multiparadigm modeling of electronic structures and dynamics., Ph.D. Thesis, California Institute of Technology, 2015.

(*19*) Feldmeier, H., and Schnack, J., (2000). Molecular dynamics for fermions. *Reviews of Modern Physics 72*, 655.

(*20*) Heller, E. J., (1975). Time-dependent approach to semiclassical dynamics. *The Journal of Chemical Physics 62*, 1544–1555.

(*21*) Frost, A. A., (1967). Floating spherical Gaussian orbital model of molecular structure. I. Computational procedure. LiH as an example. *The Journal of Chemical Physics 47*, 3707–3713.

(*22*) Su, J. T.-l., An electron force field for simulating large scale excited electron dynamics., Ph.D. Thesis, California Institute of Technology, 2007.

(*23*) Klakow, D., Toepffer, C., and Reinhard, P.-G., (1994). Semiclassical molecular dynamics for strongly coupled Coulomb systems. *The Journal of chemical physics 101*, 10766–10774.

(*24*) Kolos, W., and Wolniewicz, L., (1968). Improved Theoretical Ground-State Energy of the Hydrogen Molecule. *The Journal of Chemical Physics 49*, 404–410.

(*25*) Boothroyd, A. I., Keogh, W. J., Martin, P. G., and Peterson, M. R., (1996). A refined H3 potential energy surface. *The Journal of chemical physics 104*, 7139–7152.

(*26*) Liu, B., (1973). Ab initio potential energy surface for linear H3. *The Journal of Chemical Physics 58*, 1925–1937.

(*27*) Boothroyd, A., Martin, P., Keogh, W., Peterson, M., et al. (2002). An accurate analytic H4 potential energy surface. *Journal of Chemical Physics 116*, 666–689.

(*28*) Hemley, R., Mao, H., Finger, L., Jephcoat, A., Hazen, R., and Zha, C., (1990). Equation of state of solid hydrogen and deuterium from single-crystal x-ray diffraction to 26.5 GPa. *Physical Review B 42*, 6458.